1   **Loss of adenylyl cyclase 6 in leptin receptor expressing stromal cells attenuates loading**

2   **induced endosteal bone formation**

3

4   Mathieu Riffault[1,2,3,*], Gillian P. Johnson[1,2,3,4,*], Madeline M. Owen[1,2], Behzad Javaheri[5], Andrew

5   A. Pitsillides[5], David A. Hoey[1,2,3,4,#]

6   * Both authors contributed equally to the work

7

8   [1] Trinity Centre for Biomedical Engineering, Trinity Biomedical Sciences Institute, Trinity College

9   Dublin, Dublin, Ireland

10   [2] Department of Mechanical, Manufacturing, and Biomedical Engineering, School of Engineering,

11   Trinity College Dublin, Dublin, Ireland

12   [3] Advanced Materials and Bioengineering Research Centre (AMBER), Royal College of Surgeons

13   in Ireland and Trinity College Dublin, Dublin, Ireland

14   [4] Department of Mechanical, Aeronautical and Biomedical Engineering, University of Limerick,

15   Limerick, Ireland

16   [5] Skeletal Biology Group, Comparative Biomedical Sciences, The Royal Veterinary College,

17   London, UK

18

19   **Running title:** Adenylyl Cyclase 6 is required for load-induced bone formation

20

1

21   **Corresponding author**

22   David A. Hoey, PhD

23   Mechanical & Manufacturing Engineering, Parsons Building, Trinity College Dublin, Dublin 2,

24   Ireland

25   Telephone: +353 1 8961359

26   Email: dahoey@tcd.ie

27

28

31

2

Abstract

Bone marrow stromal/stem cells represent a quiescent cell population that replenish the osteoblast bone-forming cell pool with age and in response to injury, maintaining bone mass and repair. A potent mediator of stromal/stem cell differentiation *in vitro* and bone formation *in vivo* is physical loading, yet it still remains unclear whether loading-induced bone formation requires the osteogenic differentiation of these resident stromal/stem cells. Therefore, in this study, we utilized the Leptin Receptor (LepR) to identify and trace the contribution of bone marrow stromal cells to mechanoadaptation of bone *in vivo*. 12 week old *Lepr-cre;tdTomato* mice were subjected to compressive tibia loading with an 11N peak load for 40 cycles, every other day for 2 weeks. Histological analysis revealed that Lepr-cre;tdTomato$^+$ cells arise perinatally around blood vessels and populate bone surfaces as lining cells or osteoblasts before a percentage undergo osteocytogenesis. Lepr-cre;tdTomato$^+$ stromal cells within the marrow increase in abundance with age but not following the application of tibial compressive loading. Mechanical loading induces an increase in bone mass and bone formation parameters, yet does not evoke an increase in Lepr-cre;tdTomato$^+$ osteoblasts or osteocytes. To investigate whether adenylyl cyclase-6 (AC6) in LepR cells contributes to this mechanoadaptive response, *Lepr-cre;tdTomato* mice were further crossed with AC6$^{fl/fl}$ mice to generate a LepR$^+$ cell-specific knockout of *AC6*. These *Lepr-cre;tdTomato;AC6$^{fl/fl}$* animals have an attenuated response to compressive tibia loading, characterised by a deficient load-induced osteogenic response on the endosteal bone surface. This, therefore, demonstrates that Lepr-cre;tdTomato$^+$ cells contribute to short term bone mechanoadaptation.

Keywords: stem cells, mechanobiology, bone adaptation, *in vivo* mechanical loading, adenylyl cyclase 6

3

1. Introduction

Physical loading is a potent regulator of bone anabolism, yet the cellular mechanisms by which this occurs are not fully understood [1, 2]. This mechanoadaptive response involves bone formation by osteoblasts which are derived from a progenitor or stromal cell population. The finite lifespan of the osteoblast suggests that these cells must be continuously replenished from a progenitor population to meet the cellular demand imposed by mechanical loading; a similar recruitment process operates in response to injury [3-7]. Although load-induced stromal/stem cell differentiation can be indirectly coordinated by the osteocyte [8], a recent study has demonstrated loading-induced bone formation in a bone explant model that is independent of apparent mechanical stimulation of osteocytes [9]. This indicates that applied mechanical stimulation may directly promote bone marrow stem/stromal cells (MSCs) osteogenesis [5, 10]. However, neither the load-induced MSC differentiation to osteoblasts nor the mechanistic basis for MSC mechanosensing has been fully elucidated *in vivo*.

The establishment of a robust MSC marker is critical for their identification and lineage tracing *in vivo*. MSCs are traditionally described as plastic-adherent, colony-forming, non-hematopoietic cells which can differentiate into chondrogenic, adipogenic and osteogenic progeny [3, 11]. Furthermore, MSCs are often perivascular *in vivo*, where murine MSCs are characterized by their lack of expression of hematopoietic (CD45) and endothelial markers (TER-119) and positive expression of Platelet-Derived Growth Factor receptor alpha (PDGFRα), Stem cells antigen-1 (Sca1), CD51, CD105, CD90, Nestin, aSMA, and combinations thereof [3, 12-14]. MSCs can therefore be retrospectively identified based on the above characteristics, yet an appropriate method for their prospective identification is lacking, and hence their location and physiological functions *in vivo* have remained elusive. Recently, Leptin Receptor positive (LepR⁺) cells were

4

78 identified as being perivascular and a major source of the Stem cell fraction (Scf) within the bone

79 marrow [3, 15-19]. Additionally, these LepR^{+} cells were found to express the bone marrow MSC

80 markers PDGFRα, and CD51 and to be highly enriched for fibroblast colony-forming units (CFU-

81 F). Moreover, analyses indicated that LepR^{+} cells in the bone marrow largely overlap with Nestin,

82 an intermediate filament protein that is known as a neural stem/progenitor marker in adult bone

83 marrow [3, 20]. LepR^{+} cells not only express MSC markers but have now been shown to function

84 as the main source of new osteoblasts and adipocytes in adult bone marrow and to be recruited to

85 sites of injury to form bony ossicles that support haematopoiesis *in vivo* [3]. Also, osteogenic

86 differentiation of these cells is increased following anabolic stimulation with parathyroid hormone

87 [18]. Despite their presence in various tissues and organs [21, 22] and heterogenous nature [19],

88 these characteristics suggest that LepR^{+} cells are a suitable candidate to determine the role of early

89 progenitors in load-induced bone anabolic responses.

90 The candidature of these LepR^{+} cells as a means of prospectively identifying MSC fate is further

91 supported by recent studies highlighting a role for the more committed osteoprogenitors in load-

92 induced bone formation. Work by Liu et al. has focused on the effect of mechanical loading on

93 primitive osteoprogenitors, looking specifically at Prrx1 (Paired related homeobox 1) and Sca1

94 positive cells [7], and Zannit et al. investigated the more committed osterix (Osx) positive

95 osteoblast lineage cells [23]. Both report proliferation of these Prrx1^{+}-Sca1^{+} and Osx^{+} cells

96 following loading, however the role of Prrx1 has been predominately characterised on the

97 periosteum.

98 The osteogenic differentiation of MSCs can be directly driven by mechanical loading *in vitro* [10,

99 24]. Furthermore, we have previously demonstrated that MSCs utilize adenylyl cyclases to

100 generate cAMP as a second messenger in this mechanotransduction leading to osteogenesis [25].

101 Adenylyl cyclases (ACs) are a family of transmembrane enzymes that catalyze the cyclization of

102 adenosine triphosphate (ATP) into cyclic adenosine monophosphate (cAMP) [26]. The AC family

103 comprises nine distinct transmembrane isoforms (AC1-AC9), each with individual regulatory

104 properties and restricted expression in only a limited number of tissues [27, 28]. Specifically, AC6

105 has been shown to be expressed in skeletal cells and is required for load-induced bone formation

106 *in vivo* [29]. Interestingly, skeletally mature mice, with a global deletion of AC6, did not present

107 with a skeletal phenotype but formed significantly less bone than control mice in response to ulna

108 loading, demonstrating that AC6 mediates bone mechanoadaptation [29]. While this study clearly

109 demonstrates a role for AC6 in bone mechanobiology, given the global deletion of this enzyme,

110 the specific cell type and mechanism of action of AC6 in bone mechanoadaptation remains unclear.

111 The development of the Lepr-cre mouse model along with specific deletion with Cre-lox

112 recombination has provided a means to study the fate of these cells and the role of associated

113 molecules. While LepR+ marrow stromal cells have been shown to be critical to adult bone

114 formation, their role in mechanoadaptation is not known. Therefore this study aimed to

115 characterise the response of LepR$^+$ marrow stromal cells to load-induced bone formation, and to

116 explore whether these cells or their progeny, contribute to load-related osteogenesis. Utilising

117 *Lepr-cre;tdTomato* mice, we have demonstrated that LepR$^+$ cells arise perinatally in bone,

118 appearing perivascularly before expanding with age to undergo osteoblastic and osteocytic

119 differentiation and act as the main source of bone-forming cells. We have demonstrated that

120 loading increases tibial bone formation and has little influence on the percentage of Lepr-

121 cre;tdTomato$^+$ stromal cells within the morrow. Moreover, no significant changes in the

122 percentage of Lepr-cre;tdTomato$^+$ cells lining bone surface or osteocytes were observed,

123 suggesting that loading does not mediate the proliferation or recruitment of LepR$^+$ cells.

124   Furthermore, our data show that *AC6* deletion in LepR$^+$ cells restricts the endosteal cortical bone

125   response to loading, highlighting the contribution of LepR$^+$ cells and a critical role for AC6 in

126   bone mechanoadaptation. However, it is currently unclear whether LeprR$^+$ cells are directly

127   responsible for the anabolic bone response or LepR$^+$ cells in the marrow contribute to the actvation

128   of non-Lepr-cre;tdTomato$^+$ cells on the bone surface in a non-autonomous manner.

129

2. Materials and Methods

2.1. Mice

132   All transgenic mice were maintained in a C57BL/6 background. Transgenic mice B6.129-

133   Lepr$^{tm2(cre)Rck}$/J JAX stock #008320 [21], B6.Cg-Ct(ROSA)26Sor$^{tm9(CAG-tdTomato)Hze}$/J JAX stock

134   #007909 [30] and B6;129-Adcy6$^{tm1.1Dek}$/J JAX stock #022503 [31] were purchased from Jackson

135   Laboratories (Maine, USA), and rederived in-house. B6.129-Lepr$^{tm2(cre)Rck}$/J and B6.Cg-

136   Ct(ROSA)26Sor$^{tm9(CAG-tdTomato)Hze}$/J were crossed to generate heterozygous B6.129-Lepr$^{tm2(cre)Rck}$/J

137   and heterozygous B6.Cg-Ct(ROSA)26Sor$^{tm9(CAG-tdTomato)Hze}$/J breeding pairs. Female B6.129-

138   Lepr$^{tm2(cre)Rck}$/J::B6.Cg-Ct(ROSA)26Sor$^{tm9(CAG-tdTomato)Hze}$/J offspring heterozygous for B6.Cg-

139   Ct(ROSA)26Sor$^{tm9(CAG-tdTomato)Hze}$/J were used for all studies. This *Lepr-cre;tdTomato* mouse

140   facilitates the labelling of cells actively expressing the Leptin receptor, in addition to their progeny

141   irrespective of receptor expression. Heterozygous *Lepr-cre;tdTomato* mice were subsequently

142   crossed with B6;129-Adcy6$^{tm1.1Dek}$/J to generate animals with a knockout for *AC6* in Lepr-

143   cre;tdTomato expressing cells resulting in a *Lepr-cre;tdTomato;AC6$^{fl/fl}$* mouse. Genotyping was

144   achieved using DNA extracted from the ear and performed by Transnetyx (Cordova, TN, USA).

145   All animals were maintained in groups of 4 under specific pathogen-free conditions at 24°C ± 2°C

146 with a 12-hour light/dark cycle and were provided with water and ad libitum diets. The procedures

147 performed in this study were approved by Trinity College Dublin Animal Research Ethics

148 Committee and Health Products Regulatory Authority in Ireland.

149

150 **2.2. Histological analysis**

151 Embryos, organs, and tibiae from all groups were dissected, fixed for 12 hrs in neutral buffered

152 formalin (Sigma-Aldrich), decalcified in 10% EDTA (Sigma-Aldrich), and processed for standard

153 paraffin embedding. Transverse 10µm sections were taken from individual samples and 2 sections

154 were used in subsequent procedures. Prior to staining, sections were dewaxed and rehydrated. For

155 haematoxylin and eosin (H&E) staining, sections were stained with HARRIS Hematoxylin

156 solution (Sigma-Aldrich) for 4 min before rinsing and staining with Eosin Y solution (Sigma-

157 Aldrich) for 2 min. Sections were subsequently rehydrated and mounted using DPX (Sigma-

158 Aldrich). Slides were imaged on an Aperio Scanscope CS2 (Leica Biosystems). For

159 immunofluorescence studies, bones tissue was fixed, decalcified and cryo-embedded. Sections of

160 20µm were sliced with a cryostat. DAPI at 1:2000 in PBS (Sigma-Aldrich) was applied to all

161 samples for 5 min prior to sample mounting on glass slides using ProLong Gold mounting medium

162 (Invitrogen). Leptin receptor staining was performed after antigen retrieval with proteinase K

163 solution (20 minutes at 37° C) in a humidified chamber. Slides were then washed with PBS-Tween

164 0.5% v/v and blocked (5% BSA in PBS, 1 hour at 37° C). Slides were incubated in the primary

165 antibody against leptin receptor (1:200, AF497, RnD Systems), washed and then in secondary

166 antibody (1:500, Ab150129, Thermofisher). DAPI at 1:2000 in PBS was then applied before

167 mounting using ProLong Gold mounting medium. Imaging was performed on the Leica SP7 (Leica

168 Microsystems) scanning confocal microscope at 20x.

169

2.3. Flow cytometry

To quantify the percentage of Tomato^{+} cells in a given population, organs were harvested, minced and homogenized, and cell suspension filtered through a 70um cell strainer. After centrifugation, cell pellets were resuspended in red blood cell lysis buffer (20mM of Tris, 150mM of NH4Cl in diH20), for 5 min on ice, then washed and resuspended in 1mL flow cytometry buffer composed of PBS (Sigma-Aldrich) with 0.5% BSA (Sigma-Aldrich) and 2mM EDTA (Sigma-Aldrich, pH7.2).

Left and right tibia were isolated, and the bone marrow was flushed from the marrow cavity with 3mL Dulbecco's modified Eagle's medium (DMEM, Sigma-Aldrich). Once flushed, cells were centrifuged at 400g for 5 min and re-suspended in 1mL red blood cell lysis buffer for 5 min on ice. Cells were washed before subsequent re-suspension in 2% Phosphate Buffer Saline (PBS)-Foetal Bovine Serum (FBS) and incubated on ice for 30 min. Cells were then incubated for 30 min on ice with CD45 (CD45-BV421, 563890, 1:100, BD Biosciences) and TER-119 (TER-119-BB515, 564760, 1:100, BD Biosciences) antibodies. After washing in PBS, cells were re-suspended in 1mL flow cytometry buffer. Flow cytometry analysis was performed on a BD LSRFortessa (BD Biosciences) at medium speed and gated at 100,000 events of Tomato^{+} cells.

2.4. *In vivo* axial tibia loading

Mice at 12 weeks of age were initially anesthetised using 4% isoflurane and were then maintained at 1.5-2% isoflurane during the remainder of the procedure. The right tibia was placed between 2 cups attached to an electromagnetic loading system with feedback control (ElectroForce 5500, TA

9

191   Instruments). After an initial 2N load, a peak compressive load of 11N was applied, for 40 cycles

192   with 10 seconds of rest between each cycle, every second day, for 2 weeks as previously described

193   [32]. Left tibiae served as non-loaded internal controls. Body weight was measured at 12 weeks of

194   age and on subsequent loading days. All animals were euthanized on day 18 and prepared for either

195   dynamic histomorphometric, histological or flow cytometry analysis.

196

197   **2.5. Micro-computed tomography (μCT) analysis**

198   Mice were placed under isoflurane-induced anaesthesia as described above. Tibiae were imaged

199   by *in vivo* micro-CT (Scanco VivaCT 80; Scanco Medical AG). The cortical area was scanned

200   with a voxel size of 25 μm. Scans were performed using a voltage of 70 kVp, a current of 114 μA

201   and a 200ms integration time. A Gaussian filter (sigma = 0.8, support = 1) was used to suppress

202   noise and a global threshold of 150 was applied for analysis or cortical bone scans. The bone

203   volume, cortical area and thickness, second moment of area around major/minor (I_{min} and I_{max})

204   were quantified using scripts provided by Scanco.

205   Whole-body scans were taken for phenotypic analysis of *Lepr-cre;tdTomato;AC6$^{fl/fl}$* mice. Briefly,

206   after euthanasia, whole-body scans were performed at 15 μm voxel size. Scans were performed

207   using a voltage of 70 kVp, a current of 114 μA and a 200ms integration time. A Gaussian filter

208   (sigma = 0.8, support = 1) was used to suppress noise and a global threshold of 150 was applied to

209   generate the 3D reconstruction using scripts provided by Scanco.

210   Whole bone analysis was performed on datasets derived from CT scans using BoneJ [33] (version

211   1.4.2), an ImageJ plugin. Following segmentation and removal of fibula from the dataset, a

212   minimum bone threshold was selected using a histogram-based method in ImageJ which utilises

10

213   all pixels in a stack to construct a histogram and was further confirmed using ImageJ "threshold

214   function". A threshold of 100 was applied to all datasets to separate higher density bone from soft

215   tissues and air. This threshold was used in "Slice Geometry" function within BoneJ to calculate

216   bone cross-sectional area (CSA), second moment of area around the minor axis (I_{max}), second

217   moment of area around the major axis (I_{min}), mean thickness determined by local thickness in two

218   dimensions (Ct.Th), ellipticity and predicted resistance to torsion (J). The most proximal (0 - 15%)

219   and the most distal portions (85 - 100%) of tibial length were excluded from analysis, as these

220   regions include trabecular bone.

221

222   **2.6. Dynamic histomorphometry**

223   Mice were injected with calcein (15 mg/kg body weight; Sigma-Aldrich) on the third and sixth

224   day of loading. Left and right tibiae were isolated, cleaned of soft tissue, fixed in formalin (Sigma-

225   Aldrich) and stored in 70% EtOH for dynamic histomorphometry. The tibiae were dehydrated in

226   graded alcohol (70–100%), infiltrated with three changes of Technovit 9100 methyl methacrylate

227   (CN Technical Services Ltd), and embedded in Technovit 9100 following manufacturer

228   recommendation. Transverse sections of the embedded tibia midshaft were imaged on a Leica SP7

229   (Leica Microsystems) scanning confocal microscope. Measurements of the bone perimeter, single

230   label perimeter, double-label perimeter, and double-label area were completed with Fiji [34]

231   (version 1.6.0_24) and used to calculate mineralizing surface/bone surface (MS/BS), mineral

232   apposition rate (MAR) and bone formation rate/bone surface (BFR/BS). Measurements were taken

233   at both the endosteum and periosteum.

234

2.7. Immunofluorescence image analysis

A region of interest for cortical bone spanning 100 slices (2500µm) was selected 3mm from the tibia-fibula junction towards the tibial proximal metaphysis. Using Fiji, the length of the bone surface covered by Tomato$^+$ cells at both endosteal and periosteal surfaces, and the number of Tomato$^+$ cells embedded within bone were counted within the region of interest.

To determine if endosteal regions showing bone formation by dynamic histomorphometry correlate with regions where Tomato$^+$ cells are observed on confocal images, both sets of images were analysed with Fiji. In order to compare between different animals, the total length of the endosteum was measured and expressed in percentage (0% starting in regard of the tibial ridge, going clockwise to 100%). Locations, where one or two labels of calcein are observed, were determined and plotted against the total length of the endosteum for static and loaded bones. Then, the presence of tdTomato$^+$ cells along the endosteum was observed and plotted against the total length of the endosteum. Results were averaged and pooled in clusters of 5%.

2.8. Statistical analysis

For flow cytometry of different tissues, a one-way ANOVA analysis was performed with Tukey correction. Dynamic histomorphometry analysis of *Lepr-cre;tdTomato;AC6$^{fl/fl}$* and comparison with wild-type mice was performed with a two-way ANOVA with Tukey correction. For all other studies, unpaired two-tailed student t-test with Wilcoxon correction was employed. Data were analysed using Graph Pad Prism 8 and for gross cortical bone morphology analysis, graphs were plotted using programming language 'R', version 3.1.3 (R Foundation for Statistical Computing,

12

256 Vienna, Austria; http://www.r-project.org). The number of animals is detailed in captions with

257 each figure. In all experiments, p<0.05 was considered statistically significant.

258

259

260 **3. Results**

261 **3.1. LepR$^+$ bone marrow cells are the main source of bone forming cells on the early**

262 **endosteal surface and later periosteal surface in addition to embedded osteocytes.**

263 We first analysed the spatiotemporal expression of LepR$^+$ cells in our model. Tomato$^+$ cells were

264 identified prenatally at E19.5 in the brain and ossification zone of the radius, ulna and tibia (Figure

265 S1). The pattern of Tomato$^+$ cells was further investigated in all major organs post-natally (Figure

266 S2). H&E staining was used to investigate the anatomy of organs, and to more accurately identify

267 the location of Tomato$^+$ cells at 8- and 12-weeks of age (Figure S2 A-F). Tomato$^+$ cells were found

268 in various organs including the liver, kidney medulla, lung, spleen, and heart (Figure S2 A-B, D-

269 F). Tomato$^+$ cells increased with age, from 8- to 12-weeks, in each of these organs. Quantification

270 of cell number within each organ of the *Lepr-cre;tdTomato* mouse was performed using flow

271 cytometry at 12-weeks which further highlighted the spatial differences in Tomato$^+$ cells. At 12

272 weeks of age, Tomato$^+$ cells accounted for less than 7% of cells in each organ with the exception

273 of the liver where 38% of cells were Tomato$^+$.

274 The expression of Lepr-cre;tdTomato$^+$ cells in 8- and 12-week old mice was analyzed in greater

275 detail within the tibiae. Sagittal sections of the tibia were imaged using confocal microscopy and

276 the trabecular and cortical bone regions examined for patterns of Tomato$^+$ cell expression (Figure

277 1). Firstly, investigating the trabecular region of the tibia of 8-week old *Lepr-cre;tdTomato* mice,

13

278   revealed the presence of Tomato$^+$ cells within the marrow space between trabeculae (Figure 1Bi-

279   Cii) where these cells located around sinusoids (Figure 1 Bii). Small populations of Tomato$^+$ cells

280   were also found lining and embedded within trabecular struts (Figure 1 Bi, Ci & Dii). While

281   Tomato$^+$ cells are located perivascularly and along the bone surface, no Tomato$^+$ cells were found

282   in the growth plate (Figure 1 Di). By 12- weeks of age, the prevalence of Tomato$^+$ cells located

283   perivascularly within the trabecular bone marrow increased (Figure 1 Ei-ii), while Tomato$^+$ cells

284   also increased along and within the trabecular bone. Interestingly, at 12 weeks of age, these cells

285   along the surface of trabecular bone morphologically resembled that of osteoblasts (cuboidal) and

286   bone lining cells (flattened)(Figure 1 F, yellow arrows) suggestive of osteoblastic differentiation

287   of LepR$^+$ bone marrow stromal cells. Furthermore, the population of Tomato$^+$ cells embedded

288   within the trabecular bone (Figure 1 F, green arrows) is evidence of osteocytic differentiation.

289   Examining the cortical bone region of the tibial mid-diaphysis, a small population of Tomato$^+$ cells

290   were found perivascularly within the marrow and along the bone surface at 8-weeks of age (Figure

291   2 A). The pattern of expansion of this cell population seen in trabecular bone also holds true when

292   the cortical bone was further examined (Figure 2 B-D); at 12 weeks, Tomato$^+$ cells are found

293   perivascularly, along the endosteal surface (Figure 2 Cii & D, yellow arrow) and embedded within

294   the cortical bone (Figure 2 D, green arrows). This observation was confirmed using flow

295   cytometry, which showed that the percentage of Tomato$^+$ cells in the marrow is 3.41% ±2.50 in

296   the tibia and 3.02% ±1.98 in the femur in 12-week old mice (Figure 2 E). Furthermore,

297   LepR$^+$CD45$^-$Ter119$^-$ bone marrow stromal cells accounted for 0.16% ±0.11 of bone marrow cells

298   within the tibia (Figure 2 F). Together, these data suggest that Lepr-cre;tdTomato$^+$ bone marrow

299   stromal cells appear perivascularly, where they expand with age, are recruited to the bone surface

300   of both trabecular and cortical bone and undergo osteoblastic and osteocytic differentiation.

14

301

3.2. Tibia loading enhances endosteal and periosteal cortical bone formation

To investigate whether there are changes in the LepR$^+$ stromal cell pool and their progeny during loading-induced bone formation, a compressive load of 11N was applied to the tibia of 12-week old female *Lepr-cre*;*tdTomato* mice (Figure 3 A-C). Consistent with previous studies, our data show that tibia loading in this model leads to an anabolic response in cortical bone of *Lepr-cre;tdTomato* mice (Figure 3 D-F). Analysis of the entire tibial cortex by micro-CT reveals an increase in cross-sectional area following loading, as well as a greater cross-sectional ellipticity (Figure 3 D). The second moment of inertia around the major (I_{min}) and minor (I_{max}) axes and the predicted resistance to torsion (J) are also enhanced following the 2 weeks of loading in *Lepr-cre;tdTomato* mice (Figure S4).

Bone formation was also measured on both the endosteal and periosteal surface using dynamic histomorphometry, where right (loaded) tibiae formed significantly more bone than left (non-loaded) tibiae (Figure 3 E,F). After 2 weeks of loading, we found a significant increase in mineralised surface, mineral apposition rate and bone formation rate at both the endosteal (Figure 3 E) and periosteal surfaces (Figure 3 F). Mineralised surface, mineral apposition rate and bone formation rate were increased by 30, 20, and 79% on the endosteal surface, respectively (Figure 3 E), while on the periosteal surface mineralised surface, mineral apposition rate and bone formation rate, increased by 23, 10, and 28%, respectively (Figure 3 F).

320

3.3. Tibial loading does not influence the number of LepR$^+$ bone marrow stromal cells nor their progeny

15

323 To determine whether these load-related increases in cortical bone formation are linked to an

324 expansion and differentiation of the Lepr-cre;tdTomato$^+$ marrow stromal cell population, bone

325 marrow was flushed from the loaded and non-loaded tibiae and flow cytometry was performed to

326 assess the percentage of Tomato$^+$ cells. The percentage of Tomato$^+$ cells did not increase following

327 tibia loading when no cellular sub-groups were excluded (Figure 4 A). However, when the CD45$^+$

328 hematopoietic and TER-119$^+$ erythropoietic cells were excluded, the percentage of Tomato$^+$

329 stromal cells was found to be slightly greater (Figure 4 B). While not significant, this could be

330 indicative of a proliferative response in these primitive Tomato$^+$ cells. Interestingly, additional

331 staining of LepR (Figure S3) reveals a colocalization of the signals from tdTomato$^+$ and LepR

332 antibody only in the marrow; Tomato$^+$ cells lining bone surfaces and Tomato$^+$ osteocytes do not

333 show immunolabelling for LepR, demonstrating that they are not actively expressing LepR at the

334 time of tissue collection on D17.

335 The effect of loading on the numbers of Tomato$^+$ cells, either lining or embedded within bone,

336 which originated from LepR$^+$ stromal cells was furthered assessed using histology (Figure 4 C).

337 No change in the percentage of Tomato$^+$ cells lining the endosteal or periosteal surface or in the

338 cells embedded in the bone as osteocytes was observed in response to tibial loading (Figure 4 D).

339 The location of Tomato$^+$ cells lining the endosteal surface was further analysed and compared to

340 the location where active bone formation had been detected by dynamic histomorphometry (Figure

341 4 E). This revealed that areas of endosteal surface where active bone formation ranged from 25-

342 45%, 55-70% and 80- 95% (Figure 4 E, upper graph) failed to exhibit any correlative difference

343 in the local number of Tomato$^+$ cells (Figure 4 E, lower graph).

344 These data demonstrate that our loading protocol which increases bone formation, does not

345 significantly induce proliferation of LepR$^+$ bone marrow stromal cells. Moreover, there is no

16

346 recruitment of this cell type to the bone surface, suggestive that a re-activation of the cells already

347 present at this location are responsible for the increased load-related bone accrual response.

348

349 **3.4. LepR$^+$ cells play a role in loading-induced bone formation via an adenylyl cyclase 6**

350 **dependent mechanism**

351 To investigate whether cells derived from LepR$^+$ stromal cells play a role in load-induced bone

352 formation, we crossed the *Lepr-cre*;*tdTomato* mouse with adenylyl cyclase 6 floxed animal

353 (*AC6$^{fl/fl}$*) to generate an *AC6* knockout in Leptin receptor expressing cells and their progeny (*Lepr-*

354 *cre;tdTomato;AC6$^{fl/fl}$*). Utilising a global deletion of Adenylyl Cyclase 6, it has been previously

355 shown that AC6 is required for loading-induced bone formation [29]. However, it is unclear in

356 which cell type AC6 is mediating this response. *Lepr-cre*;*tdTomato;AC6$^{fl/fl}$* mice are healthy and

357 fertile and appeared phenotypically normal (Figure 5 A & B, Figure S5). Body weight of all mice

358 in the study increased with age, with no differences observed between *Lepr-cre*;*tdTomato* control

359 animals and *Lepr-cre;tdTomato;AC6$^{fl/fl}$* mice at any time point (Figure S5 A). On average the body

360 weights of *Lepr-cre;tdTomato* and *Lepr-cre*;*tdTomato;AC6$^{fl/fl}$* mice were not significantly different

361 at 8- or 12-weeks of age, where *Lepr-cre*;*tdTomato* mice weighed 17.0 ±0.1g and 18.9 ±0.4g at 8-

362 and 12-weeks, respectively, whereas *Lepr-cre;tdTomato;AC6$^{fl/fl}$* mice weighed 17.7 ±0.4g and 19.0

363 ±0.8g at 8- and 12-weeks, respectively (Figure S5 A). In addition, μCT analysis was conducted to

364 further examine cortical bone microarchitecture of *Lepr-cre;tdTomato;AC6$^{fl/fl}$* and *Lepr-*

365 *cre;tdTomato* mice tibiae. The total area, cortical area, cortical thickness, I_{min}, and I_{max} at the tibial

366 midshaft of *Lepr-cre;tdTomato;AC6$^{fl/fl}$* mice were not significantly different from *Lepr-*

367 *cre;tdTomato* mice (Figure 5 C). Collectively, these data indicate that there were no differences in

368 the skeletal morphology of young adult *Lepr-cre;tdTomato* and *Lepr-cre;tdTomato;AC6$^{fl/fl}$* mice.

17

369   Thus, these results suggest *Lepr-cre;tdTomato;AC6^{fl/fl}* mice do not exhibit a gross morphological

370   or skeletal phenotype, which is consistent with the *AC6* global deletion model [29].

371   As there is no skeletal phenotype following *AC6* deletion, an identical tibial loading regime was

372   applied to the *Lepr-cre;tdTomato;AC6^{fl/fl}* mice and µCT measurements were taken along the entire

373   tibia length at the end of the loading period (Figure 6 A). Interestingly, no changes were observed

374   for tibial cross-sectional area, ellipticity (Figure 6 A), thickness of the cortical bone, I_{min}, I_{max} or

375   the resistance to torsion (Figure S7) following application of load in these *Lepr-*

376   *cre;tdTomato;AC6^{fl/fl}* mice. This result demonstrates that the deletion of *AC6* in a LepR specific

377   manner prevents the load-induced cortical bone formation otherwise observed.

378   Dynamic histomorphometry was utilised to further evaluate the effect of loading on cortical bone

379   formation in *Lepr-cre;tdTomato;AC6^{fl/fl}* mice (Figure 6 B, C). No changes in mineralised surface,

380   mineral apposition rate or bone formation rate were found at the endosteal surface of tibial cortical

381   bone in *Lepr-cre;tdTomato;AC6^{fl/fl}* post-loading (Figure 6 B) which is in agreement with µCT

382   analysis. However, on the periosteal surface, loading of *Lepr-cre;tdTomato;AC6^{fl/fl}* tibia resulted

383   in an increase in mineralised surface and bone formation rate, while no change in mineral

384   apposition rate was detected (Figure 6 C).

385   This effect of loading on Tomato$^+$;AC6$^{-/-}$ cells lining and embedded within bone was furthered

386   assessed using histology (Figure 7 A). Mechanical loading did not change the percentage of

387   Tomato$^+$;AC6$^{-/-}$ cells observed in any region of the tibiae (Figure 7 B). The percentage of

388   Tomato$^+$;AC6$^{-/-}$ cells on the endosteum, periosteum and embedded within the cortical bone were

389   investigated, and no effect of loading on cell number was evident. These data demonstrate that

390   *Lepr-cre;tdTomato;AC6^{fl/fl}* animals have both an attenuated endosteal osteogenic response to

391   loading and exhibit no change in the percentage of local Lepr-cre;tdTomato$^+$ cells. This, therefore,

       18

392   indicates that LepR$^+$ cells contribute to bone formation on the endosteal surface and that adenylyl

393   cyclase 6 is required in these cells to mediate this response.

394

395   **4. Discussion**

396   Bone marrow stromal/stem cells represent a quiescent cell population that supply bone-forming

397   osteoblast cells to maintain tissue homeostasis and to facilitate repair in response to injury. A

398   potent mediator of stromal/stem cell differentiation *in vitro* and bone formation *in vivo* is

399   mechanical loading, yet it is unclear whether load-induced bone formation requires the recruitment

400   and differentiation of resident progenitor cells. Therefore, in this study, we utilized the Leptin

401   Receptor to identify and trace the contribution of bone marrow stromal cells and their progeny to

402   bone mechanoadaptation. Lepr-cre;tdTomato$^+$ cells were tracked from E19.5 through to early

403   adulthood, to find that Lepr-cre;tdTomato$^+$ cells initially appear perivascularly within the marrow,

404   perinatally, and increase in number with age, contributing to osteoblast and osteocyte populations

405   demonstrating osteogenic lineage commitment. Compressive loading of *Lepr-cre;tdTomato* tibiae

406   resulted in increased bone formation on the endosteal and periosteal surface of cortical bone.

407   Interestingly, no significant increase in the percentage of Lepr-cre;tdTomato$^+$ stromal cells within

408   the bone marrow was observed, while no significant changes in the number of Lepr-cre;tdTomato$^+$

409   cells lining the bone surface or osteocytes embedded in bone were found following loading. *AC6*

410   deletion in Lepr-cre;tdTomato$^+$ cells resulted in a reduced endocortical bone-forming response to

411   loading, demonstrating a critical role for Lepr-cre;tdTomato$^+$ cell progeny in loading-induced bone

412   formation. In summary, these data indicate that mechanical loading does not result in the

413   proliferation of Lepr-cre;tdTomato$^+$ stromal cells within the marrow nor the recruitment of these

414   cells to the bone surface, suggesting that these cells may play either a supportive role in

19

415 osteogenesis via cell non-autonomous effects or alternatively Lepr+ cells already present along the

416 bone surface are re-activated, mediating short term load-induced bone formation in a manner that

417 is dependent on AC6.

418   Leptin Receptor is expressed prenatally in bone and brain tissue and becomes widely

419 expressed in nearly all major organs postnatally. Using confocal microscopy, the expression

420 pattern of Lepr-cre;tdTomato^{+} cells was analyzed in E19.5 mice. During this late stage of gestation,

421 a limited number of Lepr-cre;tdTomato^{+} cells were found to be present only in the brain and bone

422 tissue. This is consistent with previous work that demonstrated no Lepr-cre;tdTomato^{+} cells in the

423 ossification centre of bone at E15.5 [20], and limited LepR positive cells at E19.5, indicating little

424 contribution of these cells to bone formation at these earlier stages of development [3]. The number

425 of Lepr-cre;tdTomato[+] in the metaphyseal bone marrow showed a sharp increase by postnatal day

426 P0.5 [3], and in 1-week old mice LepR^{+} cells were present throughout the bone marrow [20]. Our

427 data, in combination with previous work, suggest that Lepr-cre;tdTomato^{+} cells increase in the

428 bone marrow during bone maturation. We have also shown that Lepr-cre;tdTomato^{+} cells were

429 present within the brain at E19.5 and are found in the heart, lungs, spleen, liver and the medulla

430 region of the kidney in 8- and 12-week old animals. Further interrogation by mRNA expression

431 analysis of *LepR* in various mouse tissues also found that the heart and spleen have the lowest

432 expression of LepR, of the tissues analysed [22], which is consistent with our findings. This wide

433 expression of Leptin Receptor has considerable implications for the use of the Leptin Receptor for

434 the study of MSC behaviour in bone, particularly when combined with Cre-lox strategy for gene

435 deletion.

436 Within bone, Lepr-cre;tdTomato^{+} cells appear perivascularly in the marrow, where they are

437 recruited to the bone surface and commit to the osteogenic lineage with age. The percentage of

20

438   Lepr-cre;tdTomato^{+} cells within the tibial marrow increased between 8- and 12-weeks of age

439   suggesting an maturation-related expansion of this cell type. This increase in marrow Lepr-

440   cre;tdTomato^{+} cells was mirrored by an increase in tdTomato^{+} cells on both bone surfaces and

441   embedded with bone. Similar findings were reported by Zhou et al. where the percentage of Lepr-

442   cre;tdTomato^{+} cells making up *Col2.3*-GFP^{+} osteoblast cells increased from 10% to 81% from 6-

443   to 14-months of age [3]. This earlier study also reported that the increase found was not due to the

444   induced expression of LepR at this age, but rather the proliferation and differentiation of LepR

445   cells resident in the bone marrow [3]. Furthermore, we did not observe LepR immunolabelling in

446   cells located on the bone surface or embedded in the bone matrix in our *Lepr-cre;tdTomato* mice,

447   and studies at 15-weeks in the same mouse model have shown that tdTomato^{+} cells in the bone

448   tissue were osteocalcin- and dentin matrix protein 1 (DMP1)-expressing mature osteoblasts and

449   osteocytes, respectively [20]. Importantly, LepR mRNA was not detectable by quantitative real-

450   time PCR in the osteoblasts, suggesting that Lepr-cre;tdTomato[+] mature bone cells do not

451   autonomously express LepR, but are descendant of LepR[+] precursors [20]. Taken together, these

452   data demonstrate that the Leptin Receptor is a robust marker of MSCs *in vivo* to trace their progeny.

453   While the contribution of Lepr-cre;tdTomato^{+} cells to the adult bone formation has been

454   investigated, their contribution to load-induced bone formation has not been examined to date.

455   Herein, *in vivo* mechanical loading of *Lepr-cre;tdTomato* mouse tibia resulted in no change in the

456   percentage of Lepr-cre;tdTomato^{+} cells along the bone surface or osteocytes, suggesting that this

457   loading protocol does not initiate recruitment of Lepr-cre;tdTomato^{+} marrow cells, but instead

458   activates resident cells at the bones surface. This is close agreement with several previous

459   observations made in other models of bone loading where both early loading-related activation of

460   osteoblast metabolic activity were observed and where there was evidence for the direct

461   transformation from quiescence to bone formation in the adult periosteum following a single brief

462   period of bone loading[35, 36].

463   The loading protocol used in this study spanned two weeks in length, therefore, while loading

464   induced a trend to an increase in the percentage of Lepr-cre;tdTomato[+] marrow stromal cells, these

465   LepR^{+} progenitor cells do not contribute to bone formation within the time frame studied. Recent

466   work from Yang *et al*. also found a lack of response in this cell population following 10 days of

467   iPTH treatment in the femoral marrow [18]. Interestingly, this finding of reactivation of mature

468   cells is consistent with a study by Chow et al., where loading of the caudal vertebrae resulted in

469   reactivation of previously quiescent bone-lining cells [37]. As with the present study, the rapidity

470   with which new bone was formed following mechanical stimulation raised the potential for this

471   bone formation to occur via the reactivation of cells already along the bone surface, rather than

472   recruitment from the stem cell niche. More recently, Matic et al, demonstrated that labelled bone

473   surface cells were observed at time points extending beyond the reported lifespan for an osteoblast,

474   suggesting continuous reactivation of bone lining cells is a potential mechanism of adult bone

475   adaptation [38]. Other recent studies have reported proliferation of osteoprogenitor (Prrx1^{+}-Sca1^{+}

476   [7]) and pre-osteoblast (Osx[+] [23]) cells as a major contributor to loading-induced bone formation

477   and not the differentiation of stem cells, which further strengthens our findings.

478   The specific knockout of *AC6* in LepR^{+} cells does not induce a skeletal phenotype but results in

479   abolition of load-induced adaptive responses at the endocortical surface, demonstrating a critical

480   role for LepR^{+} cells and their progeny in bone mechanoadaptation. The absence of a basal skeletal

481   phenotype in *Lepr-cre;tdTomato;AC6^{fl/fl}* mice suggests that AC6 does not play a role in skeletal

482   development. However, the disruption of bone mechanoadaptation on the endosteal surface in

483   *Lepr-cre;tdTomato;AC6^{fl/fl}* mice demonstrates the importance of AC6 in load-induced bone

22

484   formation. At the time of loading, approximately 50% of the bone surface is covered by cells

485   derived from LepR$^+$ cells, these cells may be responsible for the anabolic bone response and this

486   is consistent with our *in vitro* studies highlighting a vital role for AC6 in MSC and mature bone

487   cell mechanotransduction [25, 29]. However, we cannot yet directly rule out the possibility that

488   LepR$^+$ cells in the marrow may contribute to the actvation of non-Lepr-cre;tdTomato$^+$ cells on the

489   bone surface in a non-autonomous manner.

490   While the response on the periosteal surface was blunted, the bone-forming response observed at

491   this location may be attributed to other non-LepR$^+$ cells potentially recruited from the periosteum

492   [39]. For example, Duchamp de Lageneste *et al*. described a population of skeletal stem cells

493   labelled by Prrx1$^+$ in the periosteum that expressed markers shown to define mouse skeletal stem

494   cells, but were negative for leptin receptor[39]. Moreover it was demonstrated by Moore *et al*.,

495   that Prrx1$^+$ cells resident in the periosteum can sense and respond to physical stimulation *in vivo*

496   and contribute to the load-induced bone formation[40]. Additional work is required to draw

497   conclusive findings, however in our experiment this LepR$^-$/Prrx1$^+$ cell population, would not be

498   targeted by the AC6 deletion, and thus may play a role in the load-induced bone-forming response

499   observed on the periosteal surface.

500   This diminished mechanoadaptive response is in agreement with work examining a global

501   knockout of *AC6*, where AC6 deletion resulted in an inhibited response to ulna loading [29], and

502   further strengthens the potential involvement of the primary cilium, to which AC6 localises, in

503   bone mechanoadaptation [41, 42]. Furthermore, as with the *Lepr-cre;tdTomato* mouse, no change

504   was found in the percentage of Lepr-cre;tdTomato$^+$ cells on the bone surface, nor embedded within

505   the bone. The lack of bone formation, and the failure of loading to induce migration of LepR$^+$ cells

506   from the marrow to the bone surface in *Lepr-cre;tdTomato;AC6$^{fl/fl}$* mice is consistent with our

23

507 hypothesis that loading induced bone formation occurs via Lepr-cre;tdTomato$^+$ cells, and that this

508 process requires AC6.

509

510 **5. Conclusion**

511 In conclusion, this study has characterised the contribution of LepR$^+$ bone marrow stromal cells to

512 bone formation during growth and in response to mechanical loading. Interestingly, although

513 LepR$^+$ stromal cells are the main source of osteoblasts and osteocytes with age, they are not

514 recruited to the bone surface in response to short-term loading. Rather, LepR$^+$ cell contribute to

515 bone formation either through a supportive role via cell non-autonomous effects or alternatively

516 LepR$^+$ cells already present along the bone surface are re-activated. Interestingly, this activation

517 required AC6 which has previously been shown to be an important component of stem cell and

518 mature bone cell mechanotransduction.

519

24

530

531 **Author's roles**

536

537

538 **References**

539 [1] H.M. Frost, Skeletal structural adaptations to mechanical usage (SATMU): 1. Redefining

540 Wolff's law: the bone modeling problem, Anat Rec 226(4) (1990) 403-13.

541 [2] L.B. Meakin, J.S. Price, L.E. Lanyon, The Contribution of Experimental in vivo Models to

542 Understanding the Mechanisms of Adaptation to Mechanical Loading in Bone, Front Endocrinol

543 (Lausanne) 5 (2014) 154.

544 [3] B.O. Zhou, R. Yue, M.M. Murphy, J.G. Peyer, S.J. Morrison, Leptin-receptor-expressing

545 mesenchymal stromal cells represent the main source of bone formed by adult bone marrow, Cell

546 Stem Cell 15(2) (2014) 154-68.

547 [4] D. Park, J.A. Spencer, B.I. Koh, T. Kobayashi, J. Fujisaki, T.L. Clemens, C.P. Lin, H.M.

548 Kronenberg, D.T. Scadden, Endogenous bone marrow MSCs are dynamic, fate-restricted

549 participants in bone maintenance and regeneration, Cell Stem Cell 10(3) (2012) 259-72.

550 [5] E. Stavenschi, M.N. Labour, D.A. Hoey, Oscillatory fluid flow induces the osteogenic lineage

551 commitment of mesenchymal stem cells: The effect of shear stress magnitude, frequency, and

552 duration, J Biomech 55 (2017) 99-106.

553 [6] M.N. Knight, K.D. Hankenson, Mesenchymal Stem Cells in Bone Regeneration, Adv Wound

554 Care (New Rochelle) 2(6) (2013) 306-316.

555 [7] C. Liu, P. Cabahug-Zuckerman, C. Stubbs, M. Pendola, C. Cai, K.A. Mann, A.B. Castillo,

556 Mechanical Loading Promotes the Expansion of Primitive Osteoprogenitors and Organizes Matrix

557 and Vascular Morphology in Long Bone Defects, J Bone Miner Res 34(5) (2019) 896-910.

558 [8] R.T. Brady, F.J. O'Brien, D.A. Hoey, Mechanically stimulated bone cells secrete paracrine

559 factors that regulate osteoprogenitor recruitment, proliferation, and differentiation, Biochem Bioph

560 Res Co 459(1) (2015) 118-123.

561 [9] K.J. Curtis, T.R. Coughlin, D.E. Mason, J.D. Boerckel, G.L. Niebur, Bone marrow

562 mechanotransduction in porcine explants alters kinase activation and enhances trabecular bone

563 formation in the absence of osteocyte signaling, Bone 107 (2018) 78-87.

564 [10] E. Stavenschi, M.A. Corrigan, G.P. Johnson, M. Riffault, D.A. Hoey, Physiological cyclic

565 hydrostatic pressure induces osteogenic lineage commitment of human bone marrow stem cells: a

566 systematic study, Stem Cell Res Ther 9(1) (2018) 276.

567   [11] P. Bianco, P.G. Robey, P.J. Simmons, Mesenchymal stem cells: revisiting history, concepts,

568   and assays, Cell Stem Cell 2(4) (2008) 313-9.

569   [12] S. Morikawa, Y. Mabuchi, Y. Kubota, Y. Nagai, K. Niibe, E. Hiratsu, S. Suzuki, C. Miyauchi-

570   Hara, N. Nagoshi, T. Sunabori, S. Shimmura, A. Miyawaki, T. Nakagawa, T. Suda, H. Okano, Y.

571   Matsuzaki, Prospective identification, isolation, and systemic transplantation of multipotent

572   mesenchymal stem cells in murine bone marrow, J Exp Med 206(11) (2009) 2483-96.

573   [13] N. Nakao, T. Nakayama, T. Yahata, Y. Muguruma, S. Saito, Y. Miyata, K. Yamamoto, T.

574   Naoe, Adipose tissue-derived mesenchymal stem cells facilitate hematopoiesis in vitro and in vivo:

575   advantages over bone marrow-derived mesenchymal stem cells, Am J Pathol 177(2) (2010) 547-

576   54.

577   [14] C.K. Chan, E.Y. Seo, J.Y. Chen, D. Lo, A. McArdle, R. Sinha, R. Tevlin, J. Seita, J. Vincent-

578   Tompkins, T. Wearda, W.J. Lu, K. Senarath-Yapa, M.T. Chung, O. Marecic, M. Tran, K.S. Yan,

579   R. Upton, G.G. Walmsley, A.S. Lee, D. Sahoo, C.J. Kuo, I.L. Weissman, M.T. Longaker,

580   Identification and specification of the mouse skeletal stem cell, Cell 160(1-2) (2015) 285-98.

581   [15] L. Ding, T.L. Saunders, G. Enikolopov, S.J. Morrison, Endothelial and perivascular cells

582   maintain haematopoietic stem cells, Nature 481(7382) (2012) 457-62.

583   [16] L. Ding, S.J. Morrison, Haematopoietic stem cells and early lymphoid progenitors occupy

584   distinct bone marrow niches, Nature 495(7440) (2013) 231-5.

585   [17] R. Caire, B. Roche, T. Picot, C.M. Aanei, Z. He, L. Campos, M. Thomas, L. Malaval, L. Vico,

586   M.H. Lafage-Proust, Parathyroid Hormone Remodels Bone Transitional Vessels and the Leptin

587   Receptor-Positive Pericyte Network in Mice, J Bone Miner Res 34(8) (2019) 1487-1501.

588   [18] M. Yang, A. Arai, N. Udagawa, L. Zhao, D. Nishida, K. Murakami, T. Hiraga, R. Takao-

589   Kawabata, K. Matsuo, T. Komori, Y. Kobayashi, N. Takahashi, Y. Isogai, T. Ishizuya, A.

590   Yamaguchi, T. Mizoguchi, Parathyroid Hormone Shifts Cell Fate of a Leptin Receptor-Marked

591   Stromal Population from Adipogenic to Osteoblastic Lineage, J Bone Miner Res 34(10) (2019)

592   1952-1963.

593   [19] A.N. Tikhonova, I. Dolgalev, H. Hu, K.K. Sivaraj, E. Hoxha, A. Cuesta-Dominguez, S. Pinho,

594   I. Akhmetzyanova, J. Gao, M. Witkowski, M. Guillamot, M.C. Gutkin, Y. Zhang, C. Marier, C.

595   Diefenbach, S. Kousteni, A. Heguy, H. Zhong, D.R. Fooksman, J.M. Butler, A. Economides, P.S.

596   Frenette, R.H. Adams, R. Satija, A. Tsirigos, I. Aifantis, The bone marrow microenvironment at

597   single-cell resolution, Nature 569(7755) (2019) 222-228.

27

598 [20] T. Mizoguchi, S. Pinho, J. Ahmed, Y. Kunisaki, M. Hanoun, A. Mendelson, N. Ono, H.M.
599 Kronenberg, P.S. Frenette, Osterix marks distinct waves of primitive and definitive stromal
600 progenitors during bone marrow development, Dev Cell 29(3) (2014) 340-9.

601 [21] J. DeFalco, M. Tomishima, H. Liu, C. Zhao, X. Cai, J.D. Marth, L. Enquist, J.M. Friedman,
602 Virus-assisted mapping of neural inputs to a feeding center in the hypothalamus, Science
603 291(5513) (2001) 2608-13.

604 [22] H. Fei, H.J. Okano, C. Li, G.H. Lee, C. Zhao, R. Darnell, J.M. Friedman, Anatomic
605 localization of alternatively spliced leptin receptors (Ob-R) in mouse brain and other tissues, Proc
606 Natl Acad Sci U S A 94(13) (1997) 7001-5.

607 [23] H.M. Zannit, M.J. Silva, Proliferation and Activation of Osterix-Lineage Cells Contribute to
608 Loading-Induced Periosteal Bone Formation in Mice, JBMR Plus 3(11) (2019) e10227.

609 [24] E. Stavenschi, M.N. Labour, D.A. Hoey, Oscillatory fluid flow induces the osteogenic lineage
610 commitment of mesenchymal stem cells: The, effect of shear stress magnitude, frequency, and
611 duration, Journal of Biomechanics 55 (2017) 99-106.

612 [25] G.P. Johnson, E. Stavenschi, K.F. Eichholz, M.A. Corrigan, S. Fair, D.A. Hoey, Mesenchymal
613 stem cell mechanotransduction is cAMP dependent and regulated by adenylyl cyclase 6 and the
614 primary cilium, J Cell Sci 131(21) (2018) jcs.222737.

615 [26] M. Kamenetsky, S. Middelhaufe, E.M. Bank, L.R. Levin, J. Buck, C. Steegborn, Molecular
616 details of cAMP generation in mammalian cells: a tale of two systems, J Mol Biol 362(4) (2006)
617 623-39.

618 [27] J. Hanoune, N. Defer, Regulation and role of adenylyl cyclase isoforms, Annual review of
619 pharmacology and toxicology 41 (2001) 145-74.

620 [28] N. Defer, M. Best-Belpomme, J. Hanoune, Tissue specificity and physiological relevance of
621 various isoforms of adenylyl cyclase, Am J Physiol Renal Physiol 279(3) (2000) F400-16.

622 [29] K.L. Lee, D.A. Hoey, M. Spasic, T. Tang, H.K. Hammond, C.R. Jacobs, Adenylyl cyclase 6
623 mediates loading-induced bone adaptation in vivo, FASEB J 28(3) (2014) 1157-65.

624 [30] L. Madisen, T.A. Zwingman, S.M. Sunkin, S.W. Oh, H.A. Zariwala, H. Gu, L.L. Ng, R.D.
625 Palmiter, M.J. Hawrylycz, A.R. Jones, E.S. Lein, H. Zeng, A robust and high-throughput Cre
626 reporting and characterization system for the whole mouse brain, Nat Neurosci 13(1) (2010) 133-
627 40.

28

628   [31] K.P. Roos, K.A. Strait, K.L. Raphael, M.A. Blount, D.E. Kohan, Collecting duct-specific

629   knockout of adenylyl cyclase type VI causes a urinary concentration defect in mice, Am J Physiol

630   Renal Physiol 302(1) (2012) F78-84.

631   [32] R.L. De Souza, M. Matsuura, F. Eckstein, S.C. Rawlinson, L.E. Lanyon, A.A. Pitsillides,

632   Non-invasive axial loading of mouse tibiae increases cortical bone formation and modifies

633   trabecular organization: a new model to study cortical and cancellous compartments in a single

634   loaded element, Bone 37(6) (2005) 810-8.

635   [33] M. Doube, M.M. Klosowski, I. Arganda-Carreras, F.P. Cordelieres, R.P. Dougherty, J.S.

636   Jackson, B. Schmid, J.R. Hutchinson, S.J. Shefelbine, BoneJ: Free and extensible bone image

637   analysis in ImageJ, Bone 47(6) (2010) 1076-9.

638   [34] J. Schindelin, I. Arganda-Carreras, E. Frise, V. Kaynig, M. Longair, T. Pietzsch, S. Preibisch,

639   C. Rueden, S. Saalfeld, B. Schmid, J.Y. Tinevez, D.J. White, V. Hartenstein, K. Eliceiri, P.

640   Tomancak, A. Cardona, Fiji: an open-source platform for biological-image analysis, Nat Methods

641   9(7) (2012) 676-82.

642   [35] R.A. Dodds, N. Ali, M.J. Pead, L.E. Lanyon, Early loading-related changes in the activity of

643   glucose 6-phosphate dehydrogenase and alkaline phosphatase in osteocytes and periosteal

644   osteoblasts in rat fibulae in vivo, J Bone Miner Res 8(3) (1993) 261-7.

645   [36] M.J. Pead, T.M. Skerry, L.E. Lanyon, Direct transformation from quiescence to bone

646   formation in the adult periosteum following a single brief period of bone loading, J Bone Miner

647   Res 3(6) (1988) 647-56.

648   [37] J.W. Chow, A.J. Wilson, T.J. Chambers, S.W. Fox, Mechanical loading stimulates bone

649   formation by reactivation of bone lining cells in 13-week-old rats, J Bone Miner Res 13(11) (1998)

650   1760-7.

651   [38] I. Matic, B.G. Matthews, X. Wang, N.A. Dyment, D.L. Worthley, D.W. Rowe, D. Grcevic, I.

652   Kalajzic, Quiescent Bone Lining Cells Are a Major Source of Osteoblasts During Adulthood, Stem

653   Cells 34(12) (2016) 2930-2942.

654   [39] O. Duchamp de Lageneste, A. Julien, R. Abou-Khalil, G. Frangi, C. Carvalho, N. Cagnard,

655   C. Cordier, S.J. Conway, C. Colnot, Periosteum contains skeletal stem cells with high bone

656   regenerative potential controlled by Periostin, Nat Commun 9(1) (2018) 773.

657   [40] E.R. Moore, Y. Yang, C.R. Jacobs, Primary cilia are necessary for Prx1-expressing cells to

658   contribute to postnatal skeletogenesis, J Cell Sci 131(16) (2018).

659   [41] E.R. Moore, J.C. Chen, C.R. Jacobs, Prx1-Expressing Progenitor Primary Cilia Mediate Bone

660   Formation in response to Mechanical Loading in Mice, Stem Cells Int 2019 (2019) 3094154.

661   [42] J.C. Chen, D.A. Hoey, M. Chua, R. Bellon, C.R. Jacobs, Mechanical signals promote

662   osteogenic fate through a primary cilia-mediated mechanism, FASEB J 30(4) (2016) 1504-11.

663

8- and 12 -week-old *Lepr-cre;tdTomato* mice tibia. tdTomato⁺ cells / DAPI

664
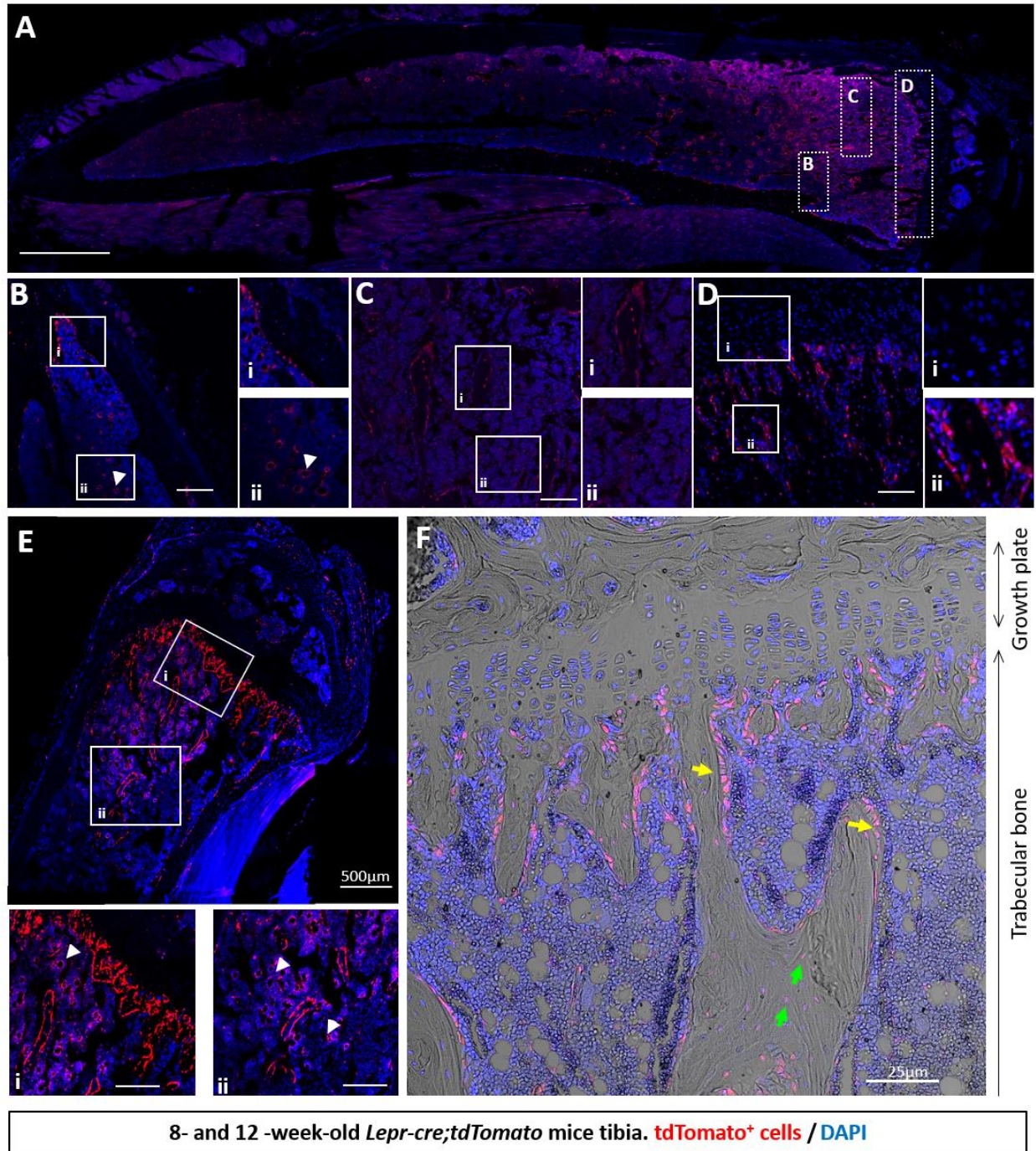
Figure 1: tdTomato[+] bone marrow cells appear around sinusoids and contribute to osteoblast and osteocyte populations over time in trabecular bone. To assess whether *LepR-cre* was actively expressed in adult tibia, limbs were harvested from 8- and 12-week-old *Lepr*-cre*;tdTomato* mice and processed for histological analyses with the nuclear dye DAPI. **(A)** Representative image of

31

669   an 8-week old tibia, showing regions of interest. **(B-D)** Confocal microscopy revealed tdTomato$^+$

670   signal in 8-week old trabecular bone marrow **(B-Bi)**, perivascularly in the marrow space (arrow

671   head; Bii), in trabecular bone **(C)**, and below the growth plate **(D)**. **(Di)** No staining was found in

672   the growth plate. **(E-F)** Confocal microscopy revealed tdTomato$^+$ signal in 12-week old mice along

673   the trabecular bone **(E)** and in trabecular bone marrow **(Ei-ii)**. **(Ei-ii)** tdTomato$^+$ was found to be

674   perivascular in the marrow space (arrow head). **(F)** No staining was found in the growth plate.

675   Additionally, tdTomato$^+$ is expressed on the bone surface (yellow arrow) and embedded within

676   bone (green arrow) in 12-week old mice. n=4. Scale bar 50µm unless otherwise indicated.
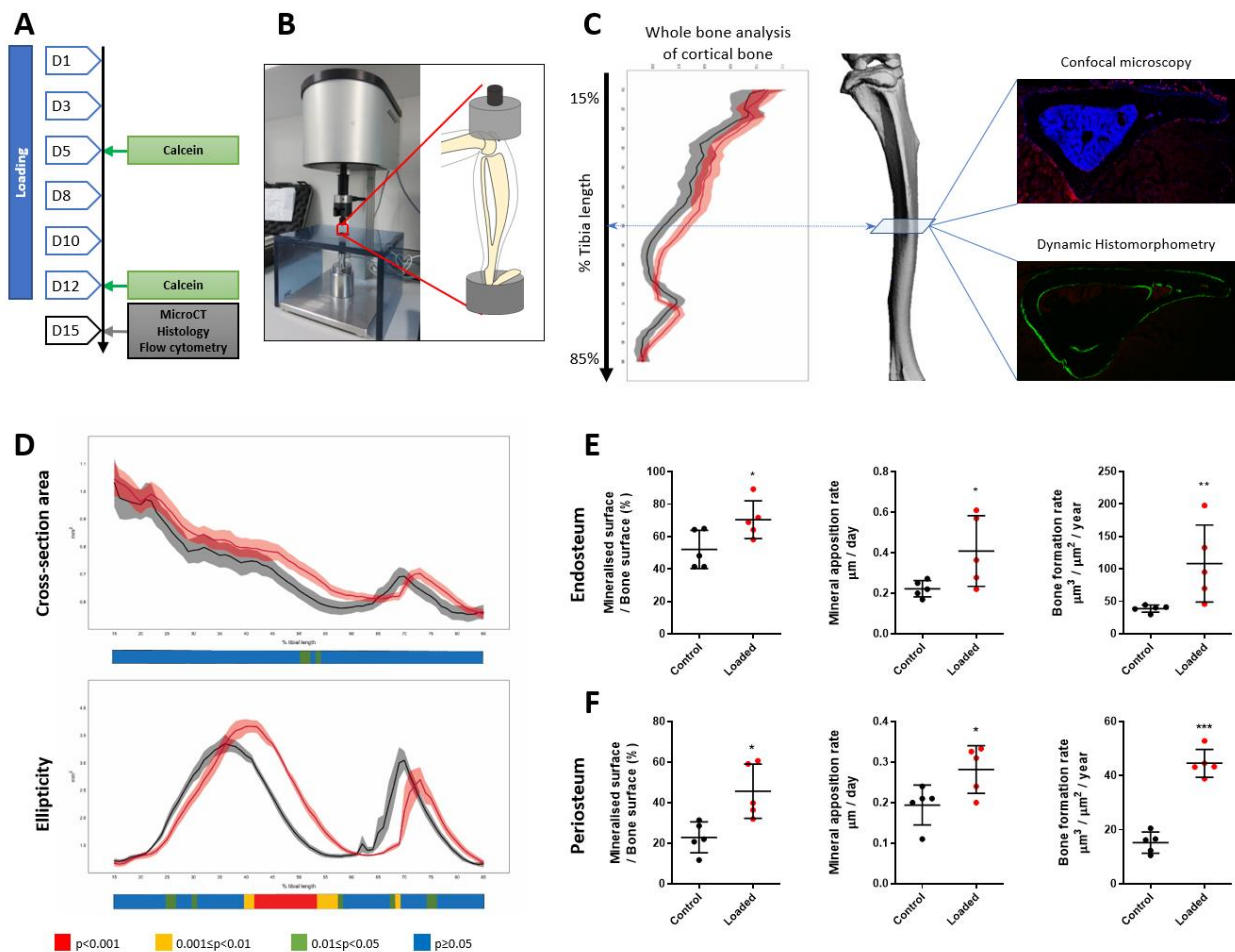
8- and 12 -week-old *Lepr-cre;tdTomato* mice tibia. tdTomato⁺ cells / DAPI
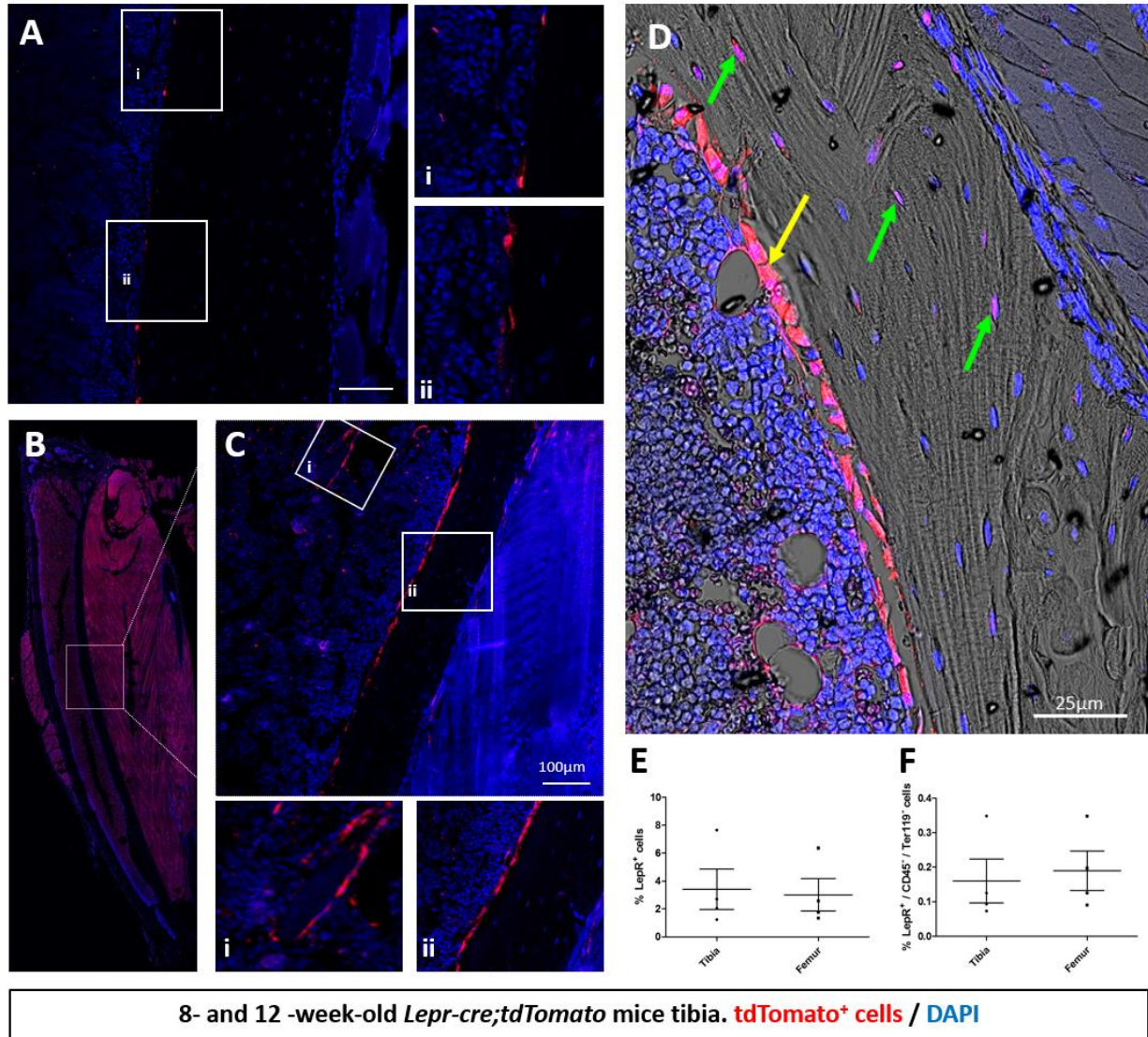
Figure 2: tdTomato⁺ bone marrow cells appear around sinusoids and contribute to osteoblast and osteocyte populations over time in cortical bone. To assess whether *LepR-cre* was actively expressed in adult tibia, limbs were harvested from 8- and 12-week-old mice. *Lepr-cre;tdTomato* mice and processed for histological analyses with the nuclear dye DAPI. **(A)** tdTomato⁺ signal was found on the endosteal surface of cortical bone at 8-weeks. **(B-D)** Representative image of a 12-week old tibia. **(Ci-ii)** Confocal microscopy revealed LepR signal perivascularly in the marrow space **(Ci)** and along the cortical bone surface **(Cii)**. **(D)** LepR is expressed on the bone surface

685 (yellow arrow) and embedded within bone (green arrow). n=4. Scale bar 50µm. **(E)** Flow

686 cytometry analyses revealed that in 12-week-old mice tdTomato$^+$ make up 1.23-7.65% and 1.35-

687 6.36% of bone marrow cells in the tibia and femur, respectively. **(F)** Exclusion of CD45/Ter119$^+$

688 cells reveals 0.07-0.35% and 0.09-0.34% tdTomato$^+$ cells in the tibia and femur, respectively. n=3,

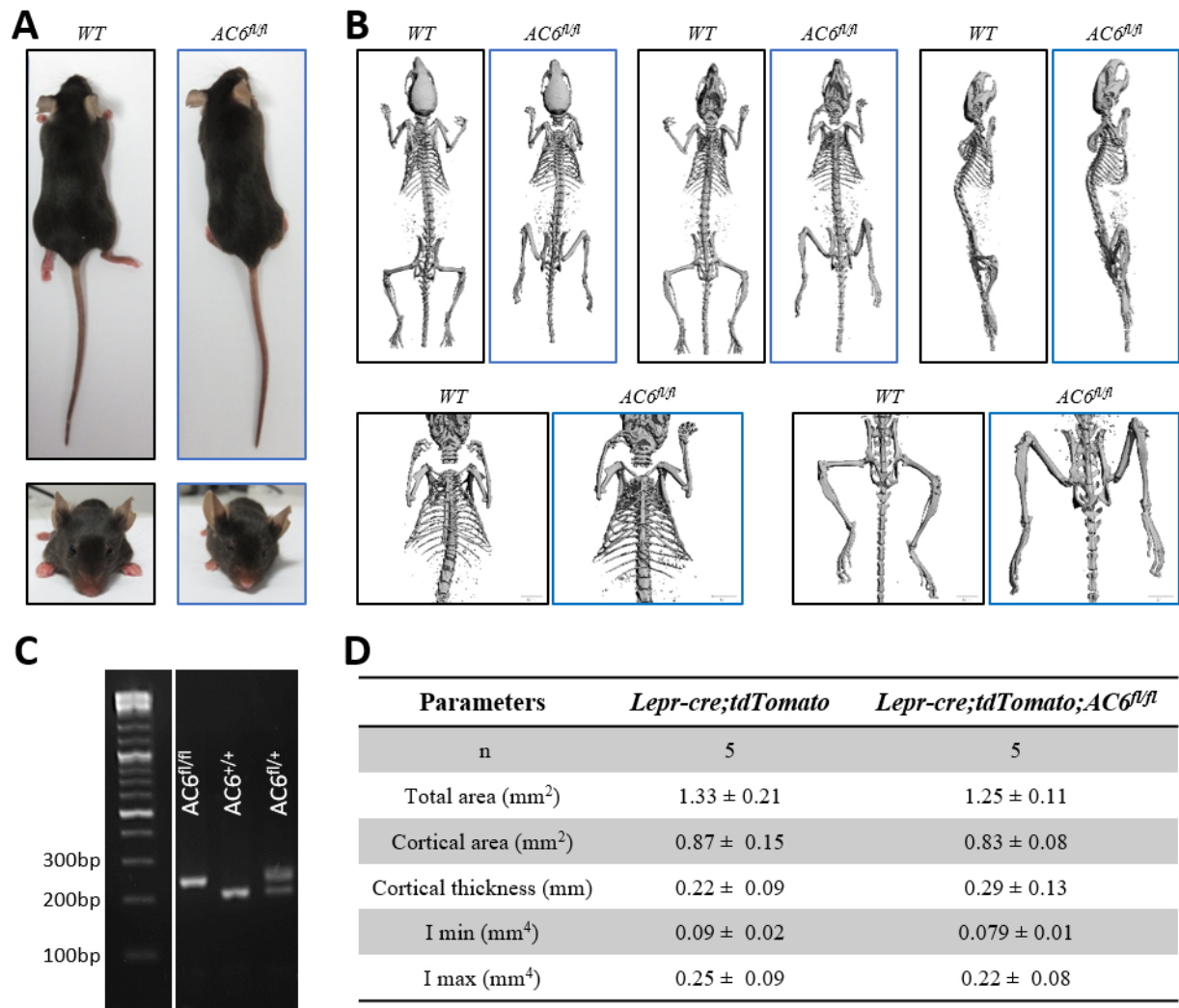689 Values are percentages +/- SD.

690

691

692 **Figure 3:** Axial tibia loading of 12-week-old *Lepr*-cre*;tdTomato* mice. **(A)** Schematic of the

693 experimental plan and tibia loading set up. **(B)** The right tibia of 12 week old mice was axially

694 loaded at 11N for 40 cycles with 10 sec rest periods per day for a total of 14 days. The left tibia

34

695   were not loaded and used as non-loaded internal controls. **(C)** Schematic representation of analyses

696   done on tibia. Whole bone microCT was performed and cortical bone analysed between 15 and

697   90% of the total tibial length, confocal microscopy on cryosections and dynamic

698   histomorphometry were performed on cross-section located between 45-50% of the tibial length.

699   **(D)** Whole bone analyses of cortical bone between 15-85% of the total tibial length, excluding

700   proximal and distal methaphyseal bone showing cross sectional area and ellipticity. Loaded: red,

701   static: black, line graph represent means +/-SEM, n=7. Statistical significance of differences along

702   the entire tibial shaft is represented as a heat map, red $p < 0.001$, yellow $0.001 \leq p < 0.01$, green

703    $0.01 \leq p < 0.05$ and blue $p \geq 0.05$. **(E-F)** Dynamic histomorphometry analysis of tibia transverse

704   section reveals tibial compressive loading enhances endosteal and periosteal cortical bone

705   formation. Relative mineralizing surface over bone surface, mineral apposition rate, and bone

706   formation rate at the endosteal **(E)** and periosteal **(F)** surface of mechanically loaded tibia. n=5.

707   Mean +/-SD.

708

36
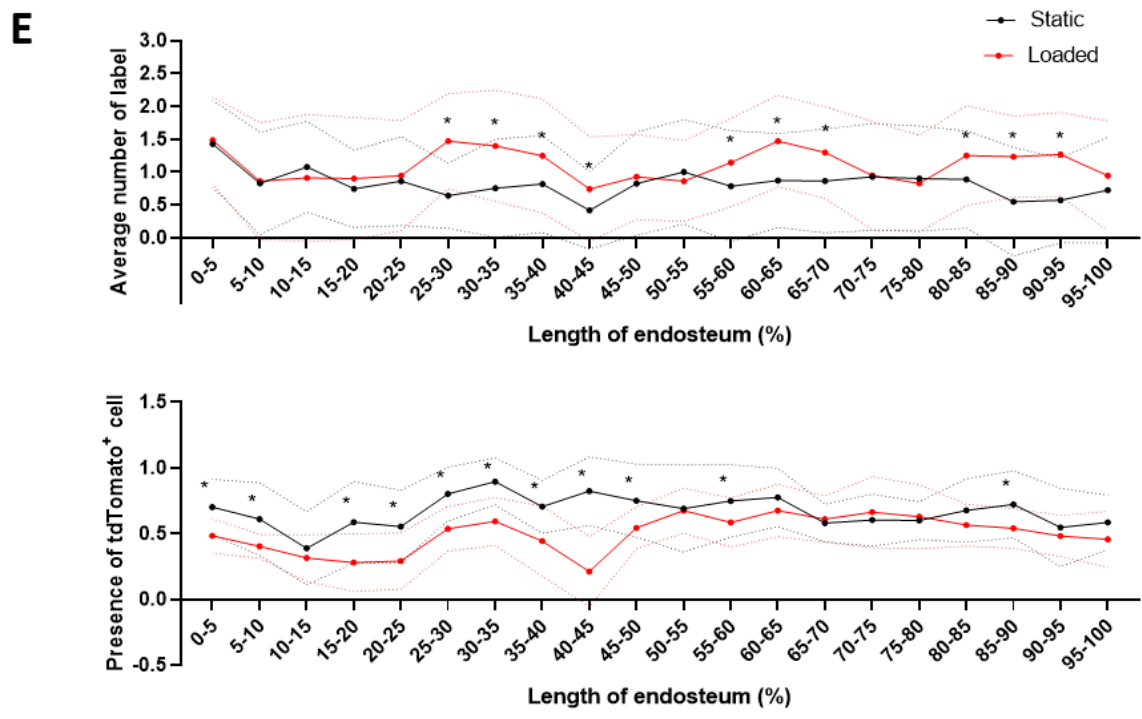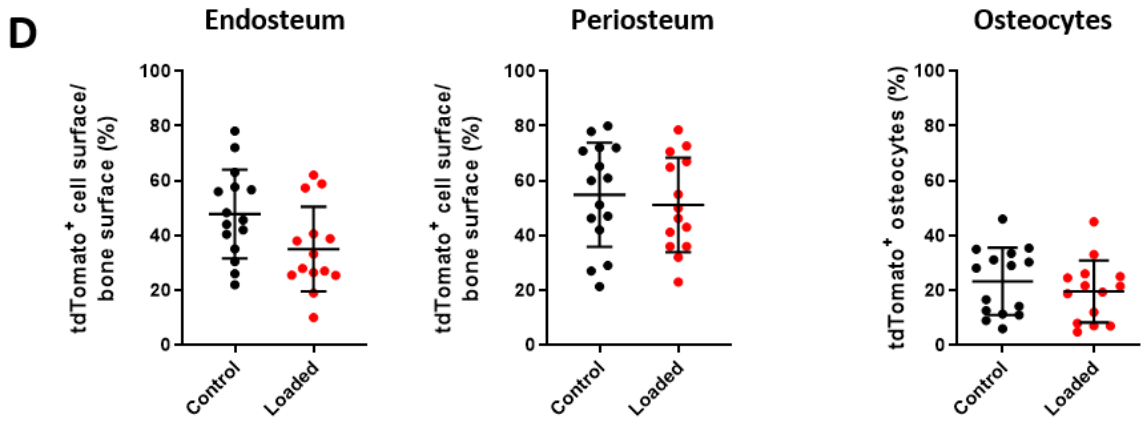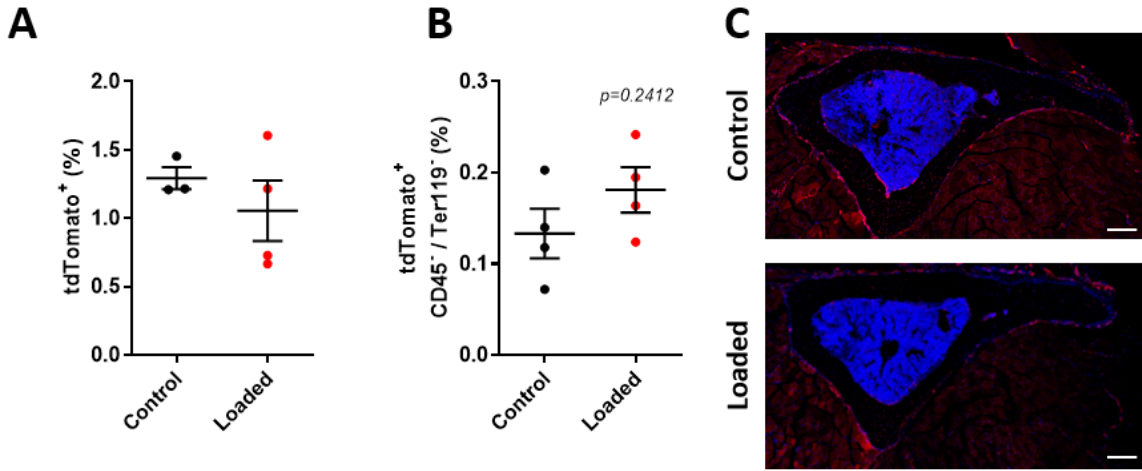
709 **Figure 4:** Tibial compressive loading doesn't alter proliferation nor location of Lepr-cre;tdTomato

710 cells. **(A-B)** Flow cytometry analyses of bone marrow cells following mechanical loading of *Lepr-*

711 cre*;tdTomato* mouse tibia. **(A)** Flow cytometry analyses revealed loading did not alter the

712 percentage of tdTomato$^+$ cells. **(B)** Exclusion of CD45$^+$ and Ter119$^+$ cells reveals a trend towards

713 an increase in tdTomato$^+$ cells following tibia loading, n=4. **(C-D)** Tibial compressive loading

714 doesn't alter the location of tdTomato$^+$ cells. **(C)** Representative image of tibia transection, scale

715 bar 100µm. **(D)** The percentage of tdTomato$^+$ cells on the endosteal or periosteal surface and

716 embedded with the bone was not altered in cortical bone following tibia compressive loading. n=7

717 **(E)** Analysis of the location of bone formation along the surface of the endosteum, upper graph:

718 average number of label observed by dynamic histomorphometry (n=4), lower graph: average

719 number of tdTomato$^+$ cells observed lining endosteum surface on confocal images (n=3).

720 Statistical tests employed unpaired two tailed student t-test. Mean +/- SD *P<0.05

37

A WT $AC6^{fl/fl}$

B WT $AC6^{fl/fl}$ WT $AC6^{fl/fl}$ WT $AC6^{fl/fl}$

WT $AC6^{fl/fl}$ WT $AC6^{fl/fl}$

C

D

Parameters	*Lepr-cre;tdTomato*	*Lepr-cre;tdTomato;AC6$^{fl/fl}$*
n	5	5
Total area (mm^2)	1.33 ± 0.21	1.25 ± 0.11
Cortical area (mm^2)	0.87 ± 0.15	0.83 ± 0.08
Cortical thickness (mm)	0.22 ± 0.09	0.29 ± 0.13
I min (mm^4)	0.09 ± 0.02	0.079 ± 0.01
I max (mm^4)	0.25 ± 0.09	0.22 ± 0.08

721

Figure 5: Phenotypic analysis of *Lepr-cre;tdTomato* and *Lepr-cre;tdTomato;AC6$^{fl/fl}$* mice at 8 and 12 weeks. **(A)** Photographs of *Lepr-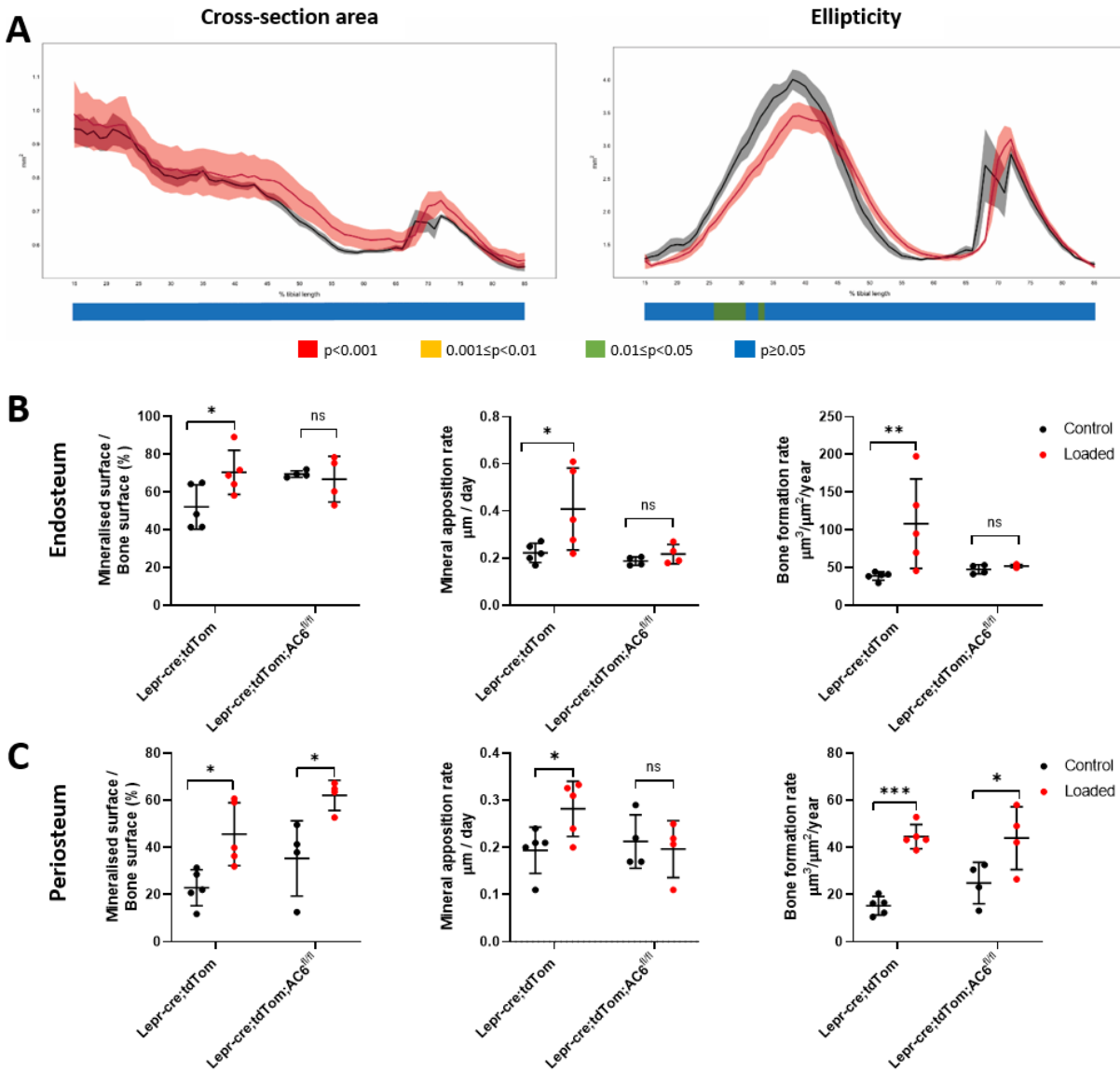cre;tdTomato* and *Lepr-cre;tdTomato;AC6$^{fl/fl}$* mice at 12-weeks old. **(B)** Full body µCT scans comparing the two genotypes. **(C)** Gel electrophoresis of genotyping showing a band at 260bp for *AC6* floxed gene. **(D)** Cortical bone midshaft geometry of 12 weeks old of *Lepr-cre;tdTomato* and *Lepr-cre;tdTomato;AC6$^{fl/fl}$* mice.

727

728

38

729

Figure 6: Axial tibia loading of 12-week-old *Lepr-cre;tdTomato;AC6^{fl/fl}* mice. **(A)** Whole bone

analyses of cortical bone of mice lacking AC6 between 15-85% of the total tibial length, excluding

proximal and distal methaphyseal bone showing cross sectional area and ellipticity. Loaded: red,

static: black, line graph represent means +/-SEM, n=6. Statistical significance of differences along

the entire tibial shaft is represented as a heat map, red $p < 0.001$, yellow $0.001 \leq p < 0.01$, green

$0.01 \leq p < 0.05$ and blue $p \geq 0.05$. **(B-C)** Mice lacking AC6 demonstrated poor mineralization on the

endosteal surface, indicated by a lack of labelling at the endosteal surface in both loaded and non-

737   loaded tibia. **(B)** Relative mineralizing surface over bone surface, mineral apposition rate and bone

738   formation rate at the endosteal surface of mechanically loaded tibia. **(C)** Relative mineralizing

739   surface over bone surface, mineral apposition rate and bone formation rate at the periosteal surface.

740   n=5 for *Lepr-cre;tdTomato*. n=3 for *Lepr-cre;tdTomato;AC6$^{fl/fl}$* . Mean +/-SD.

40

A

Control

Loaded

B

Endosteum

Periosteum

Osteocytes

C

741

41
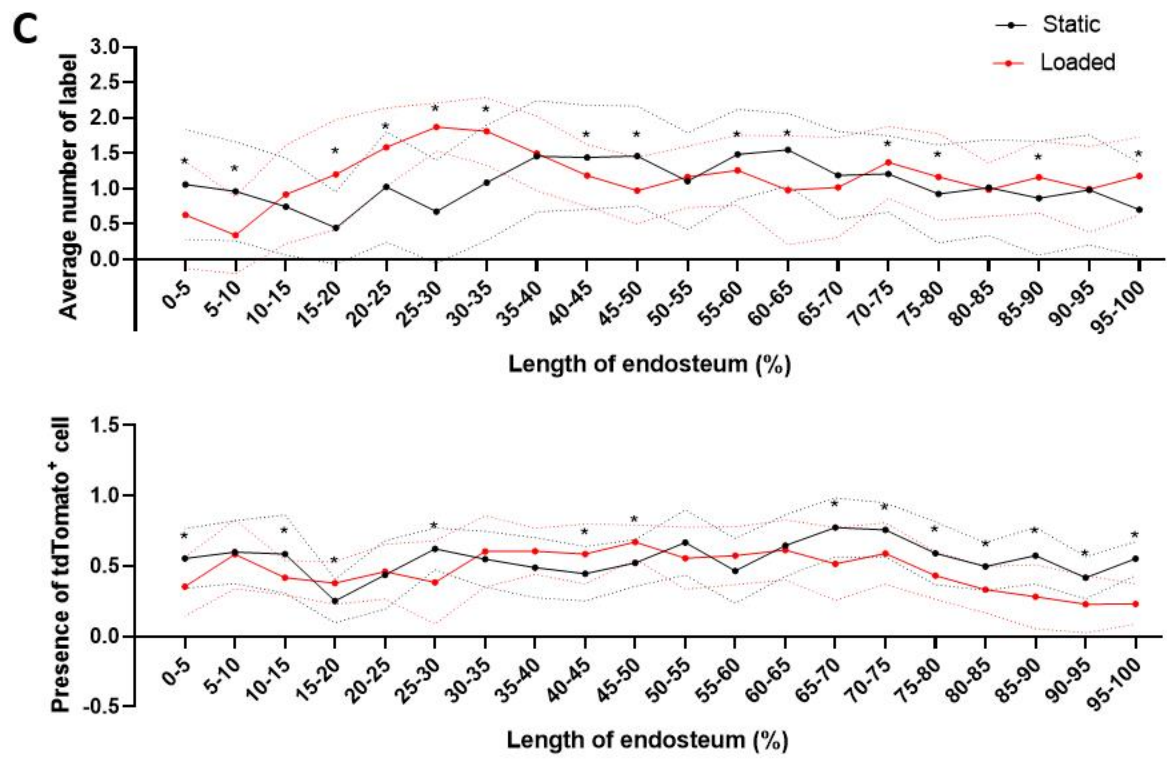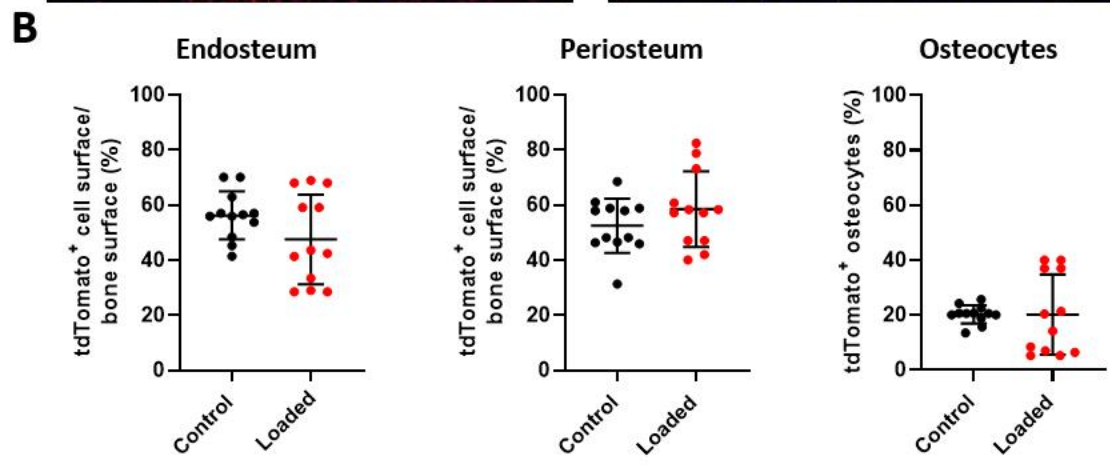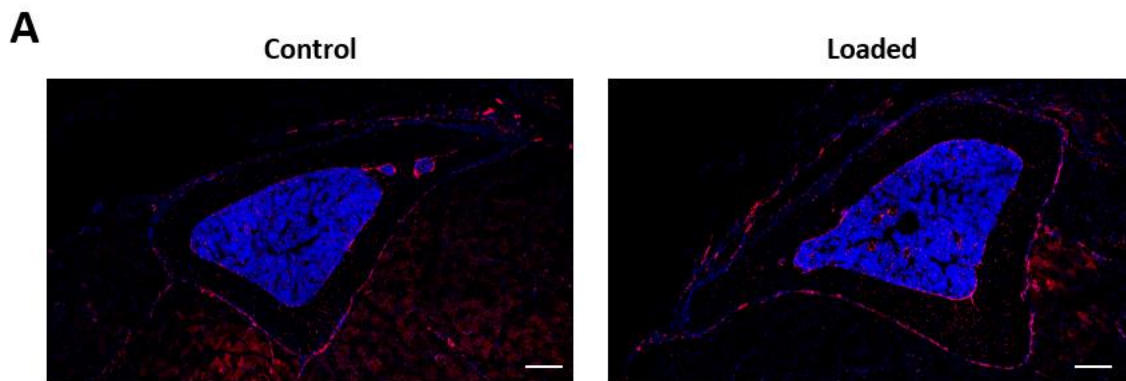
742 **Figure 7:** Tibial compressive loading doesn't alter proliferation nor location of Lepr-cre;tdTomato

743 cells in *Lepr-cre;tdTomato* and *Lepr-cre;tdTomato;AC6$^{fl/fl}$* mice. **(A)** Representative image of tibia

744 transection of *Lepr-cre;tdTomato;AC6$^{fl/fl}$* mice following tibia compressive loading, scale bar

745 100µm. **(B)** The percentage of tdTomato$^+$ cells on the endosteal, periosteal surface and embedded

746 with the bone was not altered in cortical bone. n=4. Statistical tests employed unpaired two tailed

747 student t-test with Wilcoxon correction. Mean +/- SD. **(C)** Analysis of the location of bone

748 formation along the surface of the endosteum, upper graph: average number of label observed by

749 dynamic histomorphometry (n=4), lower graph: average number of tdTomato$^+$ cells observed

750 lining endosteum surface on confocal images (n=3). Statistical tests employed unpaired two tailed

751 student t-test. Mean +/- SD *P<0.05